Relativistic mean-field approach for Λ, Ξ, and Σ hypernuclei

Z.-X. Liu (刘子鑫),[1] C.-J. Xia (夏铖君),[2] W.-L. Lu (吕万里),[1] Y.-X. Li (李玉晓),[1]
J. N. Hu (胡金牛),[3,*] and T.-T. Sun (孙亭亭)[1,†]

[1]*School of Physics and Engineering, Zhengzhou University, Zhengzhou 450001, China*
[2]*School of Information Science and Engineering, Ningbo Institute of Technology, Zhejiang University, Ningbo 315100, China*
[3]*School of Physics, Nankai University, Tianjin 300071, China*

(Received 26 May 2018; published 22 August 2018)

We systematically study the properties of single-Λ, Ξ, and Σ hypernuclei within the framework of relativistic mean-field model. The YN coupling constants are constrained according to the experimental data and previous theoretical efforts. By adding a hyperon to ^{40}Ca, we investigate its mean-field potentials, single-hyperon levels, density distributions, and binding energies, where the consequences of introducing different types of hyperons (Λ, $\Xi^{0,-}$, and $\Sigma^{+,0,-}$) are examined. In general, the Λ and Σ^0 hyperons show similar behaviors in bulk properties since both of them are electroneutral and have similar coupling constants; Ξ^0 hyperon owns the shallowest mean-field potential well with the most extended density distribution; and Coulomb interactions play vital roles in the charged Ξ^-, Σ^-, and Σ^+ hyperons. As a result, those hyperons have different impurity effects on the nuclear core ^{40}Ca. The ωYY tensor couplings are included and show remarkable effects on the spin-orbit splitting which even change the level ordering of Ξ hyperon. Finally, the single-hyperon binding energy of hypernuclei generally increases with the mass number. However, there is a turning point for Σ^+ hypernuclei at ${}^{91}_{\Sigma^+}$Nb where the binding energy begins to decrease. This is mainly due to the increasing Coulomb repulsive potential at large proton numbers.

DOI: 10.1103/PhysRevC.98.024316

I. INTRODUCTION

Hypernuclei consist of neutrons, protons, and hyperons (e.g., Λ, Σ, and Ξ hyperons), which have an additional strangeness degree of freedom compared with ordinary nuclei. Since the first Λ hypernucleus was discovered in 1953 [1], the study of hypernuclei has attracted worldwide interest in both experimental observations [2–4] and theoretical calculations [5]. An important goal in the investigations of hypernuclei is to extract information on baryon-baryon interaction, which is crucial to understand the hypernuclear structure [6–9] and neutron star properties [10–14]. Because of the difficulties in the hyperon-nucleon (YN) and hyperon-hyperon (YY) scattering experiments, there exists very few YN scattering data and no YY scattering data at all.

In the aspect of experiments, many large facilities, such as the European Organization for Nuclear Research (CERN), Brookhaven National Laboratory (BNL), Jefferson Laboratory (JLab), High Energy Accelerator Research Organization (KEK), Japan Proton Accelerator Research Complex (J-PARC), and Mainz Microtron (MAMI), have been producing a lot of hypernuclei data to investigate the strangeness nuclear physics [2–4]. The most extensively studied hypernuclear system is the single-Λ hypernucleus and rich experimental events ranging from ${}^{3}_{\Lambda}$H to ${}^{208}_{\Lambda}$Pb have been obtained in laboratories [2,15,16]. However, for Σ hypernuclei, it is generally recognized that bound Σ-hypernuclear systems do not exist except for ${}^{4}_{\Sigma}$He, which was produced in the $(K^-_{\rm stop},\pi^-)$ reaction at KEK [17]. For the hypernuclei with strangeness number $S=-2$, the experimental data are very limited because of the difficulty of the high-intensity medium-energy K^- beams required to produce such objects. Until now, three double-Λ hypernuclei, ${}^{6}_{\Lambda\Lambda}$He [18], ${}^{10}_{\Lambda\Lambda}$Be [19], and ${}^{13}_{\Lambda\Lambda}$Be [20], have been identified and the observed positive ΛΛ bond energies $\Delta B_{\Lambda\Lambda}=B_{\Lambda\Lambda}-2B_{\Lambda}$ suggest slightly attractive ΛΛ interaction. Meanwhile, there are several observed data on the Ξ hypernuclei in the ${}^{12}_{\Xi}$Be $({}^{11}\mathrm{B}+\Xi^-)$ [21], ${}^{13}_{\Xi}$B $({}^{12}\mathrm{C}+\Xi^-)$ [22], and ${}^{15}_{\Xi}$C $({}^{14}\mathrm{N}+\Xi^-)$ [23] systems. In particular, the Kiso event with the process of $\Xi^-+{}^{14}\mathrm{N}\rightarrow{}^{10}_{\Lambda}\mathrm{Be}+{}^{5}_{\Lambda}\mathrm{He}$ provided the first clear evidence of a deeply bound state of the Ξ^--^{14}N system by an attractive ΞN interaction [23].

In theoretical calculations, great efforts have been made to study the hypernuclei as a many-body system. Since hyperons do not suffer from the Pauli blocking by nucleons, they can penetrate into the nuclear interior and form deeply bound hypernuclear states. As an impurity, the hyperons may induce many effects on the nuclear core, such as the shrinkage effect [24–26], deformation [27–32], modification of cluster structure [33–35], shift of neutron drip line [36], halo structures [33,37,38], and spin and pseudospin symmetries [39–43]. Many approaches such as the cluster model [24,25,44,45], the shell model [46–48], the antisymmetrized molecular dynamics [49], the mean-field approaches [28–30,50–60], quark mean-field model [12], and *ab initio* methods [61] have contributed a lot to the investigations of the structure of hypernuclei and obtained great successes. Among these

*hujinniu@nankai.edu.cn
†ttsunphy@zzu.edu.cn

theoretical methods, the mean-field approaches can be globally applied from light to heavy hypernuclei, like Skyrme-Hartree-Fock (SHF) [28,50–53] and the relativistic mean-field (RMF) models [29,30,54–60].

During the past decades, the RMF model was very successful at describing the properties of ordinary nuclei [62–71]. Those successes quite naturally inspired attempts to describe the more general baryon systems with the strangeness degree of freedom within the same framework. In 1977, Brockmann and Weise first applied this approach to hypernuclei [54]. At that time, it had been already observed experimentally that the spin-orbit splittings in hypernuclei are significantly smaller than those in ordinary nuclei [72]. The relativistic approach is suitable for a discussion of spin-orbit splittings, which naturally emerged within the relativistic framework. As a result, the RMF model has been applied to describe single- and multi-Λ systems, including the single-particle (s.p.) spectra of Λ hypernuclei and the spin-orbit splittings, and extended beyond the Λ hyperon to other strangeness baryons [7,56,73–80].

In this work, we aim to investigate the properties of single-Λ, Ξ, and Σ hypernuclei systematically within the framework of the RMF model. Proper YN interactions will be adopted. First, by adding a hyperon to the nuclear core ^{40}Ca, the properties such as the mean-field potentials, s.p. levels, and density distributions for hyperons will be presented. The impurity effects from different hyperons on the binding energy and radius of nuclear core will be analyzed. Second, the ωYY tensor coupling effects on the hyperon spin-orbit splittings will be investigated. Finally, the mass dependence of the single-hyperon binding energies will be discussed.

The paper is organized as follows. In Sec. II, we present the RMF model for the single-Λ, Σ, and Ξ hypernuclei. After the numerical details in Sec. III, we present the results and discussions in Sec. IV. Finally, a summary is drawn in Sec. V.

II. THEORETICAL FRAMEWORK

The starting point of the meson-exchange RMF model for hypernuclei is the covariant Lagrangian density

$$\mathscr{L} = \mathscr{L}_N + \mathscr{L}_Y, \tag{1}$$

where $\mathscr{L}_N$ is the standard RMF Lagrangian density for the nucleon [62–67], in which the couplings between nucleons and the scalar σ, vector ω_μ, and vector-isovector $\vec{\rho}_\mu$ mesons and the photon A_μ are included.

The Lagrangian density $\mathscr{L}_Y$ is the contribution from the hyperons. In this work, hypernuclei with the single-Λ, Ξ, and Σ hyperon are studied and the properties of those hyperons are listed in Table I. For the electroneutral Λ hyperon with isospin 0, only the couplings with σ and ω mesons are included; for the Ξ and Σ hyperons, the couplings with σ, ω, and ρ mesons and photon are included. The Lagrangian density $\mathscr{L}_Y$ reads [57]

$$\mathscr{L}_Y = \bar{\psi}_Y\Big[i\gamma^\mu\partial_\mu - M_Y - g_{\sigma Y}\sigma - g_{\omega Y}\gamma^\mu\omega_\mu - \frac{f_{\omega Y}}{2M_Y}\sigma^{\mu\nu}\partial_\nu\omega_\mu\Big]\psi_Y + \mathscr{L}_{\rho Y} + \mathscr{L}_{AY}, \tag{2}$$

TABLE I. Strangeness number S, mass M_Y (in MeV), isospin I, total angular momentum and parity J^P, and charge Q for hyperons $Y = \Lambda$, $\Xi^{0,-}$, and $\Sigma^{+,0,-}$.

	S	M_Y	I	J^p	Q
Λ	-1	1115.6	0	$(1/2)^+$	0
Ξ^0	-2	1314.9	1/2	$(1/2)^+$	0
Ξ^-	-2	1321.3	1/2	$(1/2)^+$	$-e$
Σ^+	-1	1189.4	1	$(1/2)^+$	$+e$
Σ^0	-1	1192.5	1	$(1/2)^+$	0
Σ^-	-1	1197.4	1	$(1/2)^+$	$-e$

where M_Y are the masses of hyperons and $g_{\sigma Y}$, $g_{\omega Y}$, and $g_{\rho Y}$ are the coupling constants between a hyperon and the σ, ω, and ρ mesons, respectively. The term proportional to $\frac{f_{\omega Y}}{2M_Y}$ represents the tensor coupling between hyperons with the ω field, and the last two terms $\mathscr{L}_{\rho Y}$ and $\mathscr{L}_{AY}$ describe the interaction of a hyperon with the ρ meson and Coulomb field, respectively, which should be included for the Ξ and Σ hypernuclei. For a particular hyperon, they read

$$\mathscr{L}_{\rho Y} = \begin{cases} 0, & \text{for } \Lambda, \\ -\bar{\psi}_\Xi g_{\rho\Xi}\gamma^\mu\vec{\tau}_\Xi\cdot\vec{\rho}_\mu\psi_\Xi, & \text{for } \Xi, \\ -\bar{\psi}_\Sigma g_{\rho\Sigma}\gamma^\mu\vec{\tau}_\Sigma\cdot\vec{\rho}_\mu\psi_\Sigma, & \text{for } \Sigma, \end{cases} \tag{3}$$

and

$$\mathscr{L}_{AY} = \begin{cases} 0, & \text{for } \Lambda, \\ -\bar{\psi}_\Xi e\gamma^\mu\frac{\tau_{\Xi,3}-1}{2}A_\mu\psi_\Xi, & \text{for } \Xi, \\ -\bar{\psi}_\Sigma e\gamma^\mu\tau_{\Sigma,3}A_\mu\psi_\Sigma, & \text{for } \Sigma, \end{cases} \tag{4}$$

where $\vec{\tau}_Y$ is the isospin vector with the third component $\tau_{Y,3}$,

$$\tau_{Y,3} = \begin{cases} 0, & Y = \Lambda, \\ +1,\ -1, & Y = \Xi^0,\ \Xi^-, \\ +1,\ 0,\ -1, & Y = \Sigma^+,\ \Sigma^0,\ \Sigma^-. \end{cases} \tag{5}$$

Note that, like the Λ hyperon, the electroneutral Σ^0 hyperon couples only with the σ and ω mesons due to the zero-isospin third component.

For a system with time-reversal symmetry, the spacelike components of the vector fields vanish, leaving only the time components ω_0, $\vec{\rho}_0$, and A_0. Furthermore, one can assume that the hyperon s.p. states do not mix isospin, i.e., the s.p. states are eigenstates of $\tau_{Y,3}$, and therefore only the third component of the ρ_0 meson field, $\rho_{0,3}$, survives.

With the mean-field and no-sea approximations, the s.p. Dirac equations for baryons and the Klein-Gordon equations for mesons and photon can be obtained by the variational procedure. In the spherical case, the Dirac spinor can be expanded as

$$\psi(\boldsymbol{r}) = \frac{1}{r}\begin{pmatrix} iG_{n\kappa}(r) \\ F_{\tilde{n}\kappa}(r)\,\boldsymbol{\sigma}\cdot\hat{\boldsymbol{r}}\end{pmatrix}Y^l_{jm}(\theta,\phi), \tag{6}$$

where $G_{n\kappa}(r)/r$ and $F_{\tilde{n}\kappa}(r)/r$ are the radial wave functions for the upper and lower components with n and $\tilde{n}$ numbers of radial nodes, $Y^l_{jm}(\theta,\phi)$ is the spinor spherical harmonics, and

quantum number κ is defined by the angular momenta (l, j) as $\kappa = (-1)^{j+l+1/2}(j+1/2)$.

The Dirac equation for the radial wave functions of the hyperon is

$$\begin{pmatrix} V+S & -\frac{d}{dr}+\frac{\kappa}{r}+T \\ \frac{d}{dr}+\frac{\kappa}{r}+T & V-S-2M_Y \end{pmatrix}\begin{pmatrix} G \\ F \end{pmatrix} = \varepsilon \begin{pmatrix} G \\ F \end{pmatrix}, \quad (7)$$

where ε is the s.p. energy. For a particular hyperon, the scalar potential S, vector potential V, and ωYY tensor potential T are

$$S = g_{\sigma Y}\sigma, \quad \text{for } \Lambda, \Xi, \text{ or } \Sigma, \quad (8a)$$

$$V = \begin{cases} g_{\omega\Lambda}\omega_0, & \text{for } \Lambda, \\ g_{\omega\Xi}\omega_0 + g_{\rho\Xi}\tau_{\Xi,3}\rho_{0,3} + e\frac{\tau_{\Xi,3}-1}{2}A_0, & \text{for } \Xi, \\ g_{\omega\Sigma}\omega_0 + g_{\rho\Sigma}\tau_{\Sigma,3}\rho_{0,3} + e\tau_{\Sigma,3}A_0, & \text{for } \Sigma, \end{cases} \quad (8b)$$

and

$$T = -\frac{f_{\omega Y}}{2M_Y}\partial_r\omega_0, \quad \text{for } \Lambda, \Xi, \text{ or } \Sigma. \quad (8c)$$

The mesons and photon fields satisfy the radial Laplace equation

$$\left(-\frac{d^2}{dr^2} - \frac{2}{r}\frac{d}{dr}\right)\phi = S_\phi, \quad (9)$$

with the source terms

$$S_\phi = \begin{cases} -m_\sigma^2\sigma - g_\sigma\rho_s - g_{\sigma Y}\rho_{sY} - g_2\sigma^2 - g_3\sigma^3, & \text{for } \sigma, \\ -m_\omega^2\omega_0 + g_\omega\rho_v + g_{\omega Y}\rho_{vY} + \frac{f_{\omega Y}}{2M_Y}\partial_i j_{TY}^{0i} - c_3\omega_0^3, & \text{for } \omega_0, \\ -m_\rho^2\rho_{0,3} + g_\rho\rho_3 + g_{\rho Y}\rho_{3Y}, & \text{for } \rho_{0,3}, \\ +e\rho_c + e\rho_{cY}, & \text{for } A_0, \end{cases} \quad (10)$$

where m_ϕ ($\phi = \sigma$, ω, and ρ) are the meson masses and is zero for photon; g_σ, g_ω, g_ρ, g_2, g_3, and c_3 are the parameters of the nucleon-nucleon (NN) interaction in the Lagrangian density $\mathscr{L}_N$; $\rho_s(\rho_{sY})$, $\rho_v(\rho_{vY})$, $\rho_3(\rho_{3Y})$, and $\rho_c(\rho_{cY})$ are the radial scalar, baryon, isovector, and charge density for the nucleons (hyperons), respectively; and j_{TY}^{0i} is the tensor density for the hyperons. With the radial wave functions, these densities for the hyperons can be expressed as

$$\rho_{sY}(r) = \frac{1}{4\pi r^2}\sum_{k=1}^{A_Y}\left[\left|G_k^Y(r)\right|^2 - \left|F_k^Y(r)\right|^2\right], \quad (11a)$$

$$\rho_{vY}(r) = \frac{1}{4\pi r^2}\sum_{k=1}^{A_Y}\left[\left|G_k^Y(r)\right|^2 + \left|F_k^Y(r)\right|^2\right], \quad (11b)$$

$$j_{TY}^{0i}(r) = \frac{1}{4\pi r^2}\sum_{k=1}^{A_Y}\left[2G_k^Y(r)F_k^Y(r)\right]\boldsymbol{n}, \quad (11c)$$

$$\rho_{3Y}(r) = \frac{1}{4\pi r^2}\sum_{k=1}^{A_Y}\left[\left|G_k^Y(r)\right|^2 + \left|F_k^Y(r)\right|^2\right]\tau_{Y,3}, \quad (11d)$$

and

$$\rho_{cY}(r) = \begin{cases} \frac{1}{4\pi r^2}\sum_{k=1}^{A_\Xi}\left[\left|G_k^\Xi(r)\right|^2 + \left|F_k^\Xi(r)\right|^2\right]\frac{\tau_{\Xi,3}-1}{2}, & \text{for } \Xi, \\ \frac{1}{4\pi r^2}\sum_{k=1}^{A_\Sigma}\left[\left|G_k^\Sigma(r)\right|^2 + \left|F_k^\Sigma(r)\right|^2\right]\tau_{\Sigma,3}, & \text{for } \Sigma, \end{cases} \quad (11e)$$

where $\boldsymbol{n}$ is the angular unit vector. The hyperon number A_Y is determined by the baryon density $\rho_{vY}(r)$ as

$$A_Y = \int 4\pi r^2 dr \rho_{vY}(r). \quad (12)$$

The coupled equations (7)–(11) in the RMF model are solved numerically in the coordinate space.

As the translational symmetry is broken in the mean-field approximation, a proper treatment to the center-of-mass (c.m.) motion is very important, especially for light nuclei. In the present calculation, we employ a microscopic c.m. correction as shown in Ref. [81],

$$E_{\text{c.m.}} = -\frac{1}{2M}\langle\hat{\boldsymbol{P}}^2\rangle, \quad (13)$$

where $M = \sum_B M_B$ is the total mass of the (hyper)nucleus and $\hat{\boldsymbol{P}} = \sum_B \hat{\boldsymbol{P}}_B$ is the total momentum operator. With the c.m. correction, the total energy for a hypernucleus in RMF is finally given as

$$\begin{aligned} E_{\text{tot}} &= \sum_{k=1}^{A}\varepsilon_k + \sum_{k=1}^{A_Y}\varepsilon_k^Y \\ &- 2\pi\int r^2 dr\left[g_\sigma\rho_s\sigma + g_{\sigma Y}\rho_{sY}\sigma + \frac{1}{3}g_2\sigma^3 + \frac{1}{2}g_3\sigma^4\right] \\ &- 2\pi\int r^2 dr\left[g_\omega\rho_v\omega_0 + g_{\omega Y}\rho_{vY}\omega_0 + \frac{f_{\omega Y}}{2m_Y}\partial_i j_{TY}^{0i}\omega_0 - \frac{1}{2}c_3\omega_0^4\right] \\ &- 2\pi\int r^2 dr\left[g_\rho\rho_3\rho_{0,3} + g_{\rho Y}\rho_{3Y}\rho_{0,3} - \frac{1}{2}d_3\rho_{0,3}^4\right] \\ &- 2\pi\int r^2 dr[e\rho_c A_0 + e\rho_{cY}A_0] + E_{\text{c.m.}}. \end{aligned} \quad (14)$$

III. NUMERICAL DETAILS

In this work, the single-Λ, Σ, and Ξ hypernuclei are calculated by the RMF model. In the following, we also use the notation ${}^A_Y Z$ to represent a hypernucleus with the mass number $A = A_n + A_p + A_Y$, where A_n is the neutron number, A_p is the proton number, and A_Y is the number of embedded hyperons. For a hypernucleus with an electroneutral hyperon, the electric charge Z corresponds to the number of protons while for a hypernucleus with charged hyperons such as $\Sigma^{+,-}$ and Ξ^-, the value of Z is altered.

For the NN interaction, the effective interaction PK1 [82] is adopted, which can provide excellent descriptions not only for nuclear matter but also for finite nuclei both in and far from the valley of β stability. For the YN interaction, the sets of

TABLE II. Coupling constants $\alpha_{\sigma Y} = g_{\sigma Y}/g_{\sigma N}$, $\alpha_{\omega Y} = g_{\omega Y}/g_{\omega N}$, $\alpha_{\rho Y} = g_{\rho Y}/g_{\rho N}$, and $\alpha_{TY} = f_{\omega Y}/g_{\omega Y}$ in the YN interactions for the $Y = \Lambda$, Ξ, and Σ hyperons.

	$\alpha_{\sigma Y}$	$\alpha_{\omega Y}$	$\alpha_{\rho Y}$	α_{TY}			
Λ	0.618	0.667	0.0	0.0	−0.122	−0.541	−1.0
Ξ	0.313	0.333	1.0	0.0	−0.4	−1.89	−2.27
Σ	0.619	0.667	1.0	0.0	0.76	1.0	1.417

coupling constants $\alpha_{\sigma Y} = g_{\sigma Y}/g_{\sigma N}$, $\alpha_{\omega Y} = g_{\omega Y}/g_{\omega N}$, $\alpha_{\rho Y} = g_{\rho Y}/g_{\rho N}$, and $\alpha_{TY} = f_{\omega Y}/g_{\omega Y}$ are listed in Table II. The ΛN interaction is taken as in Ref. [83], which is fixed by reproducing the experimental single-Λ binding energy $B_\Lambda^{(1s)}$ of the $1s$ orbit in hypernucleus ${}^{40}_{\Lambda}$Ca. With this ΛN parameter, the single-Λ spectra for hypernuclei from ${}^{12}_{\Lambda}$C to ${}^{208}_{\Lambda}$Pb can be well described. The ΞN interaction is taken as in Ref. [80], which is determined by fitting the observed Ξ^- removal energy in the Kiso event related to the hypernucleus ${}^{15}_{\Xi}$C (^{14}N + Ξ^-). The ΣN interaction is taken as in Ref. [57]. In these YN interactions, the vector coupling constants $g_{\omega Y}$ are taken according to the naive quark model [84], namely,

$$g_{\omega\Lambda} = g_{\omega\Sigma} = 2g_{\omega\Xi} = \tfrac{2}{3}g_{\omega N}, \tag{15}$$

and the tensor coupling constants α_{TY} are adopted as $\alpha_{T\Lambda} = -1.0$ [83], $\alpha_{T\Xi} = -0.4$ [85], and $\alpha_{T\Sigma} = 1.0$ [84], respectively. Several other values of α_{TY}, i.e., $\alpha_{T\Lambda} = -0.122, -0.541$, $\alpha_{T\Xi} = -1.89, -2.27$, and $\alpha_{T\Sigma} = 0.76, 1.417$ [57], are also taken to investigate the ωYY tensor coupling effects on the s.p. levels.

The Dirac equation (7), the Laplace equation (9), and the densities in Eq. (11) in the RMF model are solved in the coordinate space with a box size of $R = 20$ fm and a step size of 0.1 fm.

IV. RESULTS AND DISCUSSION

A. Hypernuclei ^{40}Ca + Y

In this part, by adding a hyperon to ^{40}Ca, the mean-field potentials, single-hyperon levels, density distributions, and binding energies in the hypernuclear systems ^{40}Ca + Y ($Y = \Lambda$, Ξ, Σ) are investigated and the consequences of introducing different types of hyperons are examined.

In Fig. 1, the hyperon mean-field potentials $V + S$ and the corresponding s.p. levels in the hypernuclei ^{40}Ca + Y are presented, where $Y = \Lambda$, $\Xi^{0,-}$, and $\Sigma^{+,0,-}$. For comparison, we first set the ωYY tensor coupling constant $\alpha_{TY} = 0$ for all hypernuclei. Obvious differences in the potential depths are obtained except for the Λ and Σ^0 hyperons, with very similar mean-field potentials indicated by solid lines. This is because both the Λ and Σ^0 hyperons couple only with σ and ω mesons and have very close coupling strengths, as shown in Table II. Moreover, in Fig. 1(a), the potential depth of the Λ hyperon is about twice of the Ξ^0 hyperon, which yields fewer bound states in the Ξ^0 spectra. This is mainly due to the weaker σ-Ξ^0 and ω-Ξ^0 couplings, which are around half of σ-Λ and ω-Λ couplings. However, the Ξ^- hyperon is more deeply bound than the Ξ^0 hyperon, which is caused by the attractive Coulomb potential of Ξ^- hyperons. In Fig. 1(b), the results of Σ hyperons are presented. The effect of Coulomb interaction is very distinct. From Σ^- to Σ^+ hypernuclei, the s.p. states become almost 15 MeV less bound, and the Coulomb barrier around 5 MeV near the nuclear surface of the Σ^+ can be seen clearly.

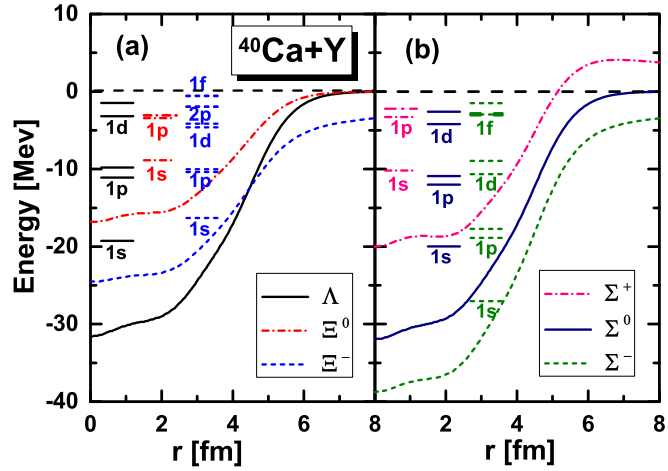

FIG. 1. Mean-field potentials $V + S$ and s.p. levels for the hyperons in the hypernuclei ^{40}Ca + Y. In panel (a), $Y = \Lambda$ and $\Xi^{0,-}$, and in panel (b), $Y = \Sigma^{+,0,-}$. $\alpha_{TY} = 0$.

In Table III, the values of the s.p. energies for the Λ, Ξ, and Σ hyperons in the hypernuclei ^{40}Ca + Y are listed. For comparison, the experimental data and corresponding theoretical results for the hypernucleus ${}^{40}_{\Lambda}$Ca are also presented. Note that the ωYY tensor coupling constant $\alpha_{T\Lambda} = -1$ for ${}^{40}_{\Lambda}$Ca while 0 for ^{40}Ca + Y. Very close single-Λ binding energies are obtained for ${}^{40}_{\Lambda}$Ca in theory and experiment, with the differences less than 5% of the experimental values. The spin-orbit splittings in the single-Λ hypernuclei ${}^{40}_{\Lambda}$Ca and ${}^{41}_{\Lambda}$Ca are commonly less than 0.3 MeV, which are in accordance with the experimental conclusion [55]. For hypernuclei ^{40}Ca + Y with electroneutral hyperons ($Y = \Lambda$, Ξ^0, Σ^0), comparing with the single-Λ spectra, the single-Ξ^0 spectra do not possess high-angular-momentum states due to the weak single-Ξ^0 potential at nuclear saturation density while the single-Σ^0 spectra are systematically more bound, which results from the smaller repulsive effect of the kinetic energy yielded by the larger M_Σ. Furthermore, compared with those electroneutral hyperons, Coulomb interaction plays an important role for charged hyperons; i.e., the s.p. spectra for the negative charged Ξ^- and Σ^- hyperons are more deeply bound, while those for the positive charged Σ^+ hyperons are weakly bound.

To understand the differences in the mean-field potentials for hyperons, in Fig. 2, we show different contributions to the total hyperon mean-field potentials $V_{\rm tot} = V + S = V_{\sigma+\omega} + V_\rho + V_C$, i.e., the contributions from the σ and ω mesons ($V_{\sigma+\omega}$), ρ meson (V_ρ), and photon (V_C).

In Fig. 2(a), only σ and ω mesons contribute to the total potential since Λ hyperon is isoscalar and electroneutral. In Figs. 2(b) and 2(c), besides the σ and ω mesons, the ρ meson and photon also contribute to the total potentials since the Ξ^- and Σ^- hyperons are isovector and charged. The contributions

TABLE III. Comparison of the s.p. energies (in MeV) for $Y = \Lambda$, $\Xi^{0,-}$, and $\Sigma^{+,0,-}$ in the hypernuclei ^{40}Ca + Y. The experimental data and corresponding theoretical results for the nearby hypernucleus $^{40}_{\Lambda}$Ca are also listed for comparison. $\alpha_{T\Lambda} = -1$ for $^{40}_{\Lambda}$Ca and $\alpha_{TY} = 0$ for ^{40}Ca + Y.

	$^{40}_{\Lambda}$Ca (Expt.)	$^{40}_{\Lambda}$Ca	^{40}Ca + Y					
			Λ	Ξ^0	Ξ^-	Σ^+	Σ^0	Σ^-
$1s_{1/2}$	-18.7 ± 1.1	-18.73	-19.26	-8.85	-16.32	-10.20	-19.98	-27.04
$2s_{1/2}$		-1.90	-1.98		-4.48		-2.93	-8.93
$1p_{3/2}$		-10.10	-11.10	-3.42	-10.38	-3.30	-12.02	-18.86
$1p_{1/2}$	-11.0 ± 0.6	-9.86	-9.80	-3.08	-10.01	-2.21	-10.89	-17.73
$2p_{3/2}$					-1.97			-3.04
$2p_{1/2}$					-1.94			-2.82
$1d_{5/2}$		-2.14	-3.18		-4.61		-4.21	-10.65
$1d_{3/2}$	-1.0 ± 0.5	-1.87	-1.46		-4.14		-2.61	-8.95
$1f_{7/2}$					-0.60			-2.97
$1f_{5/2}$					-0.54			-1.50

from $V_{\sigma+\omega}$ are very close for the Λ and Σ^- hyperons, but much larger than that for the Ξ^- hyperon, due to the smaller σ-Ξ and ω-Ξ couplings. Meanwhile, the potential $V_{\sigma+\omega}$ leads to the main difference of $V_{\rm tot}$ between the Ξ^- and Σ^- hyperons. The contributions from Coulomb potential V_C are quite similar for these negative charged hyperons.

In Fig. 3, we plot the density distributions $\rho_v(r)$ for different hyperons, i.e., $Y = \Lambda$, $\Xi^{0,-}$ in Fig. 3(a) and $Y = \Sigma^{+,0,-}$ in Fig. 3(b), in the ^{40}Ca + Y systems. In our present calculations, the single-hyperon occupies the $1s_{1/2}$ orbit. It can be easily seen that the Λ and Σ^0 hyperons have quite similar density distributions due to similar s.p. energies of their occupied $1s_{1/2}$ orbits. Compared with the Λ and Σ^0 hyperons, the density distribution for the Ξ^0 hyperon is the most diffused while that for the Σ^- hyperon is the most bound. This is because of the shallowest Ξ^0 mean-field potential while the deepest Σ^- potential. In this sense, the hyperon halo is most likely to be found in the Ξ^0 hypernuclei.

In Table IV, the total binding energy $E_{\rm tot}$, the hyperon s.p. energy ε^Y_{1s}, the energy contribution from the nuclear core $E_{\rm core}$, and the c.m. correction $E_{\rm cm}$ are listed for the single-hyperon hypernuclei $^{41}_{\Lambda}$Ca (^{40}Ca + Λ), $^{41}_{\Xi^0}$Ca (^{40}Ca + Ξ^0), $^{41}_{\Xi^-}$K (^{40}Ca + Ξ^-), $^{41}_{\Sigma^+}$Sc (^{40}Ca + Σ^+), $^{41}_{\Sigma^0}$Ca (^{40}Ca + Σ^0), and $^{41}_{\Sigma^-}$K (^{40}Ca + Σ^-). For comparison, the energies for the ordinary nucleus ^{40}Ca are also given. By comparing the total binding energies $E_{\rm tot}$ between ^{40}Ca and single-hyperon hypernuclei, it can be easily seen that the added hyperon makes the nuclear systems much more bound because of the attractive NY interactions, especially in the hypernuclei $^{41}_{\Lambda}$Ca, $^{41}_{\Sigma^0}$Ca, and $^{41}_{\Sigma^-}$K. Accordingly, the obtained single-hyperon energies ε^Y_{1s} are very large for the Λ, Σ^0, and Σ^- hyperons.

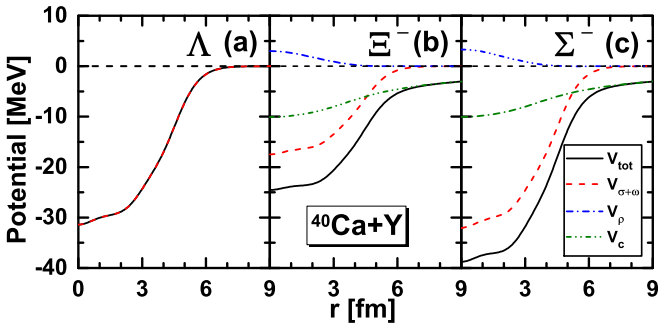

FIG. 2. Comparison of the total mean-field potentials $V_{\rm tot} = V_{\sigma+\omega} + V_\rho + V_C$ (solid curves) and various components (dashed curves) for the $Y = \Lambda$ (a), Ξ^- (b), and Σ^- (c) hyperons in the hypernuclei ^{40}Ca + Y. Potentials $V_{\sigma+\omega}$, V_ρ, and V_C are the contributions from the $\sigma + \omega$ mesons, ρ meson, and photon, respectively. $\alpha_{TY} = 0$.

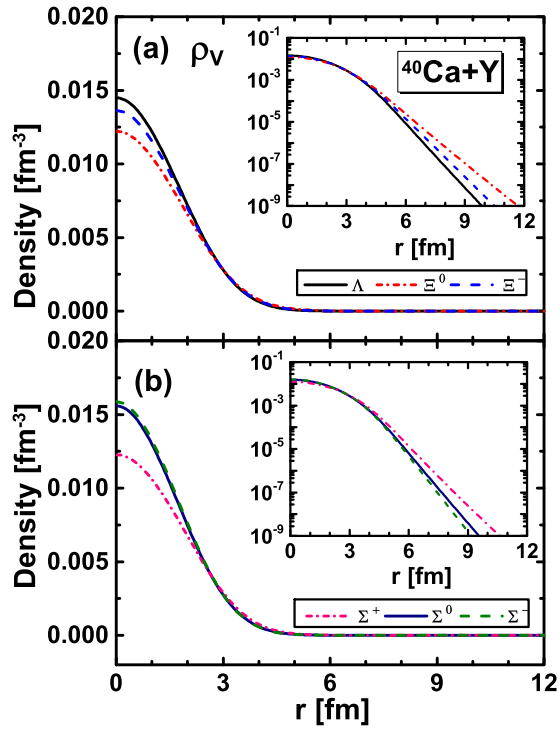

FIG. 3. Density distributions ρ_v for the hyperons in the hypernuclei ^{40}Ca + Y. In panel (a), $Y = \Lambda$ and $\Xi^{0,-}$; in panel (b), $Y = \Sigma^{+,0,-}$. The inserted figures are the same but in log scales. $\alpha_{TY} = 0$.

TABLE IV. Energies (in MeV) and radii (in fm) for the hypernuclei ^{40}Ca + Y with $Y = \Lambda$, $\Xi^{0,-}$, and $\Sigma^{+,0,-}$ by the RMF model. Energies listed are, respectively, the total binding energy $E_{\rm tot}$, the hyperon s.p. energy of $1s_{1/2}$ orbit ε^Y_{1s}, energy contributed by the nuclear core $E_{\rm core}$, and the c.m. correction $E_{\rm c.m.}$. Detailed contributions for the hyperon energy from the σ, ω, and ρ mesons and Coulomb force are presented as well, i.e., $E_{\sigma Y} = \int 4\pi r^2 dr g_{\sigma Y}\rho_{sY}\sigma$, $E_{\omega Y} = \int 4\pi r^2 dr[g_{\omega Y}\rho_{vY}\omega_0 + \frac{f_{\omega Y}}{2m_Y}\partial_i j^{0i}_{TY}\omega_0]$, $E_{\rho Y} = \int 4\pi r^2 dr g_{\rho Y}\rho_{3Y}\rho_{0,3}$, and $E^Y_{\rm cou} = \int 4\pi r^2 dr e\rho_{cY}A_0$. Radii listed are, respectively, the mass radius $R_{\rm tot}$, hyperon radius R_Y, neutron radius R_n, and proton radius R_p, calculated by $R = \sqrt{\int dr r^4\rho_v(r)/\int dr r^2\rho_v(r)}$ with the particle vector density $\rho_v(r)$ and charge radius R_c calculated by $R_c = \sqrt{R_p^2 + 0.864^2 + 0.336^2 \times \frac{N}{Z}}$. For comparison, the results for the nearby ordinary nucleus ^{40}Ca are also given. $\alpha_{TY} = 0$.

	^{40}Ca	$^{41}_{\Lambda}$Ca	$^{41}_{\Xi^0}$Ca	$^{41}_{\Xi^-}$K	$^{41}_{\Sigma^+}$Sc	$^{41}_{\Sigma^0}$Ca	$^{41}_{\Sigma^-}$K
$E_{\rm tot}$	−342.797	−361.884	−351.870	−359.615	−353.418	−362.583	−370.408
ε^Y_{1s}		−19.263	−8.852	−16.315	−10.197	−19.981	−27.039
$E_{\rm core}$	−333.860	−333.785	−334.248	−334.496	−334.434	−333.774	−334.517
$E_{\rm c.m.}$	−8.937	−8.837	−8.770	−8.804	−8.788	−8.828	−8.852
$E_{\sigma Y}$		−103.807	−49.319	−51.174	−100.403	−105.860	−107.131
$E_{\omega Y}$		91.622	42.751	44.435	88.258	93.359	94.552
$E_{\rho Y}$		0	0.207	0.665	0.203	0	0.751
$E^Y_{\rm cou}$		0	0	−4.185	4.613	0	−4.266
$R_{\rm tot}$	3.327	3.313	3.317	3.310	3.319	3.311	3.307
R_Y		2.745	2.938	2.809	2.830	2.660	2.625
R_n	3.303	3.302	3.286	3.317	3.287	3.302	3.319
R_p	3.351	3.350	3.367	3.327	3.373	3.350	3.325
R_c	3.445	3.444	3.461	3.421	3.467	3.444	3.420

The c.m. correction $E_{\rm c.m.}$ in different hypernuclei are very close, and one possible reason for their slight differences is the hyperon mass difference. After removing ε^Y_{1s} and $E_{\rm c.m.}$ from the total binding energy, the energy contributed by the nuclear core can be described, i.e., $E_{\rm core} = E_{\rm tot} - \varepsilon^Y_{1s} - E_{\rm c.m.}$. In all the hypernuclei, the nuclear core energies are very close with the difference less than 0.75 MeV. To see the detailed energy contributions for the single-hyperon energy ε^Y_{1s}, the energies contributed by the σ, ω, ρ mesons and Coulomb field are analyzed. The energy contributions from σ and ω mesons are around −7 to −12 MeV while that from ρ meson is much smaller and less than 1.0 MeV, and the Coulomb field contributes remarkable energy around ±4 MeV.

To further illustrate the bulk properties of the hypernuclei, different radii such as the mass radius $R_{\rm tot}$, hyperon radius R_Y, neutron radius R_n, proton radius R_p, and charge radius R_c are also listed in Table IV. By comparing the mass radii $R_{\rm tot}$ for nucleus ^{40}Ca and hypernuclei ^{40}Ca + Y, we find that the hyperon makes the size of the nuclear system smaller. This is in accordance with the conclusion of the larger binding energy $E_{\rm tot}$. Among all the single-hyperon hypernuclei ^{40}Ca + Y, the radius of Ξ^0 hyperon is largest because of the most weakly bound $1s_{1/2}$ orbit shown in Fig. 1. By comparing with the neutron radii R_n of nucleus ^{40}Ca and hypernuclei ^{40}Ca + Y, very different impurity effects from the hyperons on the neutron radii are shown; i.e., Ξ^0 and Σ^+ hyperons decrease R_n, Ξ^- and Σ^- hyperons increase R_n, and Λ and Σ^0 hyperons have almost no influences on R_n. Those differences are mainly caused by the isospin effects related to the couplings between different hyperons and ρ meson. For the hyperons Ξ^0 and Σ^+ with $\tau_{Y,3} = +1$, they make the neutron total mean-field potential deeper by reducing the repulsive potential V_ρ contributed from ρ meson due to the opposite sign of $\tau_{n,3} = -1$ for neutrons. However, for the hyperons Ξ^- and Σ^- with $\tau_{Y,3} = -1$, they increase the mean-field potential V_ρ and the total potential becomes shallower. Unlike the case of R_n, the Coulomb interaction is important for the proton radius R_p and charge radius R_c; e.g., the positively charged Σ^+ increases R_p and R_c while the negatively charged hyperons Ξ^- and Σ^- make them smaller. Besides, the electroneutral Ξ^0 hyperon increases R_p and R_c slightly due to the same sign of τ_3 as protons, which leads to a shallower mean-field potential for protons.

B. ωYY tensor coupling effects

In this part, we investigate the ωYY tensor coupling effects on the s.p. levels, the values of the tensor coupling constant α_{TY} are taken as in Table II. For illustration and better comparison of the role of the tensor coupling played for different hyperons, we omitted the ρ-meson couplings for the Ξ and Σ hyperons as in Ref. [57].

In Fig. 4, we present the dependence of the hyperon s.p. levels on the ωYY tensor coupling constants α_{TY}. In all the hypernuclei ^{40}Ca + Y with $Y = \Lambda$, Ξ, and Σ, the ωYY tensor couplings cause obvious changes in the spin-orbit splitting. In Fig. 4(a), the ωYY coupling reduces the Λ hyperon spin-orbit splitting. The spin-orbit splittings in the $1p$ ($1p_{1/2}$ and $1p_{3/2}$) spin doublet varies from 1.3 to 0.24 MeV with $\alpha_{T\Lambda}$ increases from 0 to −1. In Figs. 4(b) and 4(c), the energy level orders for $\Xi^{0,-}$ hyperons change with extremely large negative $\alpha_{\omega\Xi} \leqslant -1.89$. In Figs. 4(d)–4(f), different from the cases of Λ and Ξ hyperons, the ωYY tensor coupling increases the spin-orbit splitting for the Σ hyperon. For $\alpha_{T\Sigma} = 1.0$, the splittings acquire almost twice of the value for $\alpha_{T\Sigma} = 0$ for all the Σ^0, Σ^+, and Σ^- hyperons.

The different effects of ωYY tensor couplings on the splittings of Λ, Ξ, and Σ can be understood by recasting the Dirac equation (7) into a Schrödinger-like equivalent form which we

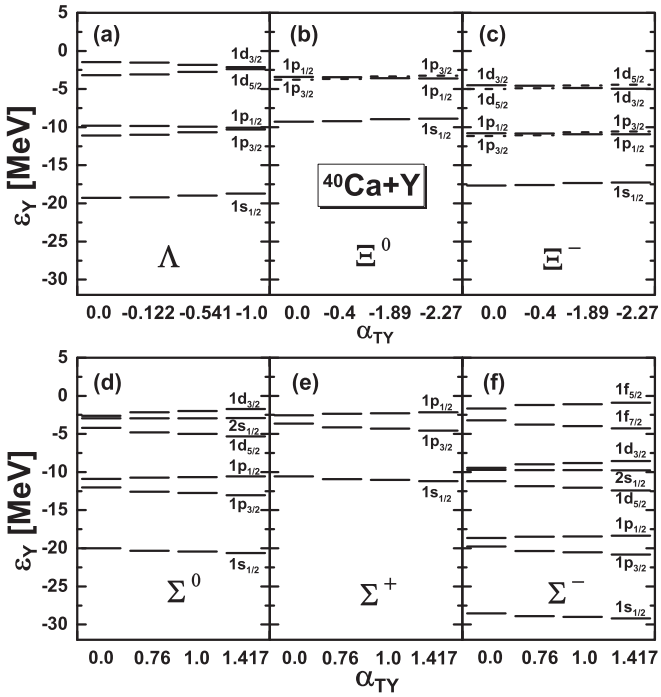

FIG. 4. Positions of the hyperon s.p. levels calculated with different ωYY tensor coupling constants α_{TY} in hypernuclei $^{40}\mathrm{Ca}+Y$ with $Y=\Lambda$ (a), $\Xi^{0,-}$ [(b), (c)], and $\Sigma^{0,+,-}$ [(d)–(f)]. The values of α_{TY} are taken as in Table II. $\alpha_{\rho Y}=0$.

can describe the spin-orbit splitting potential as [57,86]

$$V_{\mathrm{SO}}^{Y}=-\frac{1}{M_{\mathrm{eff}}}\left(\frac{1}{M_{\mathrm{eff}}}\frac{dM_{\mathrm{eff}}}{dr}+2T\right)\frac{\boldsymbol{l}\cdot\boldsymbol{s}}{r},$$
$$M_{\mathrm{eff}}=M_Y-\frac{1}{2}(V-S), \tag{16}$$

where the ωYY tensor potential $T=-\frac{\alpha_{TY}}{2M_Y}g_{\omega Y}\partial_r\omega_0$. For the Λ and Ξ hyperons, because of the negative values of α_{TY}, the ωYY tensor potential T will decrease the spin-orbit splitting potential V_{SO}^{Y} and lead to smaller spin-orbit splittings. However, for the Σ hyperon, due the positive values of α_{TY}, the tensor potential T will increase potential V_{SO}^{Y} and lead to larger spin-orbit splittings.

On the other hand, the spin-orbit splittings are very different for Λ, Ξ, and Σ hyperons in the case of $\alpha_{TY}=0$; i.e., the spin-orbit splittings for Λ and Σ hyperons are very close but much larger than those for Ξ hyperons. In this case, the spin-orbit potential $V_{\mathrm{SO}}^{Y}=-\frac{1}{M_{\mathrm{eff}}^2}\frac{dM_{\mathrm{eff}}}{dr}\frac{\boldsymbol{l}\cdot\boldsymbol{s}}{r}$ in which the hyperon effective mass M_{eff} plays the dominant role. Since the Λ and Σ hyperons own similar masses M_Y shown in Table I and mean-field potentials $V-S$ extracted from the energies $E_{\omega Y}-E_{\sigma Y}$ in Table IV, the spin-orbit potentials V_{SO}^{Y} should also be very close. However, compared with Λ and Σ hyperons, the Ξ hyperon is much more massive but has smaller values of $V-S$, which leads to much larger M_{eff} and smaller spin-orbit splittings.

In Fig. 5, the ωYY tensor potentials $T(r)$ for the Λ, Ξ^-, and Σ^- hyperons in the hypernuclei $^{40}\mathrm{Ca}+Y$ are plotted with different coupling constants α_{TY} listed in Table II. For

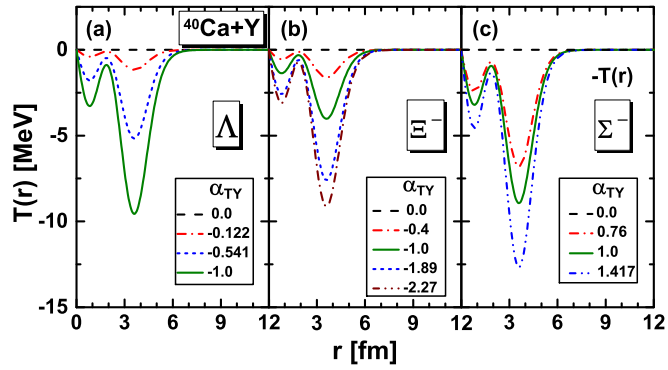

FIG. 5. Tensor potentials $T(r)$ by the ωYY couplings for the $Y=\Lambda$ (a), Ξ^- (b), and Σ^- (c) hyperons in the hypernuclei $^{40}\mathrm{Ca}+Y$ with different coupling constants α_{TY} taken from Table II. For comparison, we plot $-T(r)$ for the Σ^- hyperon. $\alpha_{\rho Y}=0$.

comparison, we also take $\alpha_{T\Xi^-}=-1$ to calculate the tensor potentials for Ξ^- hyperon. Obviously, Λ and Ξ^- hyperons own a negative ωYY tensor potential while Σ^- hyperons own a positive one, which is consistent with our previous analyses from Eq. (16). When taking $\alpha_{TY}=\pm1$, the magnitudes of the tensor potentials for both Λ and Σ^- hyperons are around 9 MeV, while a much smaller value is obtained for the Ξ^- hyperon, i.e., around 4 MeV. Besides, for the Ξ^- hyperon, varying α_{TY} from -0.4 to -1.89, the magnitudes of $T(r)$ increases significantly, which leads to the change of level ordering.

C. Mass dependence of the single-hyperon binding energies B_Y

In Fig. 6, taking hypernuclei $^{16}\mathrm{O}+Y$, $^{40}\mathrm{Ca}+Y$, $^{90}\mathrm{Zr}+Y$, and $^{208}\mathrm{Pb}+Y$ as examples, the single-hyperon binding energies B_Y for different levels versus the mass number of the hypernuclei $A^{-2/3}$ are plotted for the Λ, $\Xi^{0,-}$, and $\Sigma^{+,0,-}$ hyperons, respectively. The coupling constants $\alpha_{\sigma Y}$, $\alpha_{\omega Y}$, and $\alpha_{\rho Y}$ in the NY interactions are taken as in Table II. The ωYY tensor coupling constants for the Λ, Ξ, and Σ hyperons are taken as $\alpha_{T\Lambda}=-1$, $\alpha_{T\Xi}=-0.4$, and $\alpha_{T\Sigma}=1$, respectively. Note that the average values of B_Y for the spin doublets are adopted for the single-hyperon binding energy B_Y in Fig. 6 except the case of the s orbit.

For the Λ and Σ^0 hyperons in Figs. 6(a) and 6(d), since both of them are electroneutral with the isospin third component $\tau_{Y,3}=0$, the obtained mass dependences of the single-hyperon binding energy B_Y are very similar. As the mass number increases, the binding energy B_Y for each orbit increases and more bound levels appear. Note that there are still some differences between B_Y for Λ and Σ^0 hyperons, where the single-Σ^0 levels are more bound than those of Λ hyperons in general and one more bound orbit $1h$ appears for the Σ^0 hyperon. From O to Pb, B_Y for the $1s$ orbit increases by around 13 MeV for the Λ hyperon while around 11.5 MeV for the Σ^0 hyperon. Those differences can be attributed to the mass difference between Λ and Σ^0 hyperons and the opposite effects from the ωYY tensor couplings shown in Fig. 4.

Compared with the Λ and Σ^0 hyperons, the mass dependence of B_Y for the Ξ^0 hyperon, which is also electroneutral,

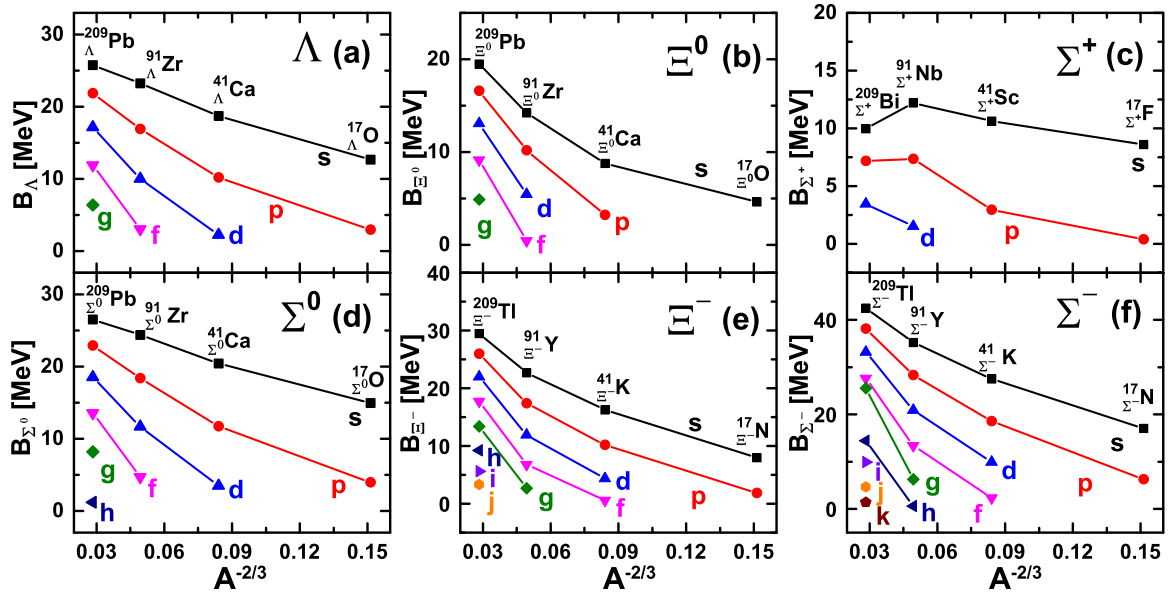

FIG. 6. Mass dependence of the single-hyperon binding energies B_Y for the hyperons $Y = \Lambda$, Σ^0 [(a), (d)], $\Xi^{0,-}$ [(b), (e)], and $\Sigma^{+,-}$ [(c), (f)] as a function of mass number $A^{-2/3}$. Coupling constants $\alpha_{\sigma Y}$, $\alpha_{\omega Y}$, and $\alpha_{\rho Y}$ in the NY interactions are taken as in Table II. The ωYY tensor coupling constants for the Λ, Ξ, and Σ hyperons are taken as $\alpha_{T\Lambda} = -1$, $\alpha_{T\Xi} = -0.4$, and $\alpha_{T\Sigma} = 1$, respectively.

is very different. On the one hand, the values of B_{Ξ^0} for all orbits are much smaller, which is mainly caused by the weaker couplings between Ξ^0 hyperon with the σ and ω mesons. On the other hand, the increase of B_Y with mass number is much more drastic for Ξ^0 hyperon, especially for the s orbit from ${}^{41}_{\Xi^0}$Ca to ${}^{209}_{\Xi^0}$Pb. This is due to large isospin effects resulting from strong coupling with ρ meson in ${}^{91}_{\Xi^0}$Zr and ${}^{209}_{\Xi^0}$Pb.

Compared with the Ξ^0 hyperon, the values of B_Y for the negatively charged Ξ^- hyperon in Fig. 6(e) are much larger due to the attractive Coulomb interaction, which leads to a considerably stronger binding of Ξ^- hyperon in the nuclear medium compared with Ξ^0 hyperon. The deepest bound state of Ξ^- in ${}^{209}_{\Xi^-}$Tl is around -29.5 MeV while that of Ξ^0 in ${}^{209}_{\Xi^0}$Pb is around -19.5 MeV. Meanwhile states with high angular momentum h, i, and j are bound in ${}^{209}_{\Xi^-}$Tl.

As in the case of Ξ^- hyperon, Coulomb interactions are also very important for the charged Σ^+ and Σ^- hyperons. As indicated in Figs. 6(c) and 6(f), the differences of B_Y for Σ^+ and Σ^- hyperons can be seen clearly. For the positively charged Σ^+ hyperon, the repulsive Coulomb interaction reduces the total binding energy drastically and only s, p, and d states are found bound in heavy hypernuclei. However, for the negatively charged Σ^- hyperon, the attractive Coulomb interaction deepens the mean-field potentials and as many as nine bound states are found. Note that this large difference from Coulomb interaction for the Σ^+ and Σ^- hyperons will be weakened slightly by their couplings with the ρ meson. Besides, in the Σ^+ hypernuclei, an abnormal mass dependence of B_Y is found in the large-mass region. From ${}^{91}_{\Sigma^+}$Nb to ${}^{209}_{\Sigma^+}$Bi, the values of B_Y decrease a lot. This is because of the stronger repulsive Coulomb potential with the increasing proton number A_p.

From Fig. 6, it can be seen that for most hyperons, the single-hyperon binding energies B_Y increase with the mass number except for the Σ^+ hyperon, which has a turning point at ${}^{91}_{\Sigma^+}$Nb where the binding energy begins to decrease. To illustrate these behaviors clearly, in Figs. 7 and 8, taking Σ^+ and Σ^- hypernuclei as examples, we plot the evolutions of the mean-field potentials in the hypernuclei ${}^{16}\mathrm{O} + Y$, ${}^{40}\mathrm{Ca} + Y$, ${}^{90}\mathrm{Zr} + Y$, and ${}^{209}\mathrm{Pb} + Y$. Potentials including the total potential $V_{\mathrm{tot}=\sigma+\omega+\rho+\mathrm{cou}}$, the contributions from the σ and ω mesons $V_{\sigma+\omega}$, the ρ meson V_ρ, and Coulomb potential V_{cou} are presented.

From Fig. 7, we find that the total mean-field potentials V_{tot} for Σ^+ hyperons become shallower from ${}^{17}_{\Sigma^+}$F to ${}^{209}_{\Sigma^+}$Bi which

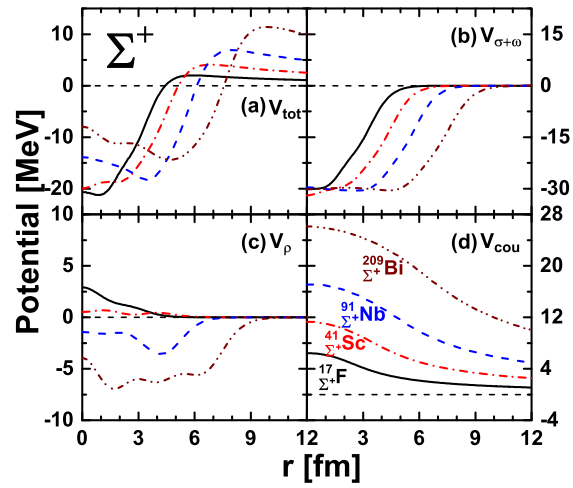

FIG. 7. Comparison of the mean-field potentials for the Σ^+ hyperons in the hypernuclei ${}^{17}_{\Sigma^+}$F, ${}^{41}_{\Sigma^+}$Sc, ${}^{91}_{\Sigma^+}$Nb, and ${}^{209}_{\Sigma^+}$Bi. Potentials presented include the total potential $V_{\mathrm{tot}} = V_{\sigma+\omega+\rho+\mathrm{cou}}$ and the potentials contributed from the σ and ω mesons $V_{\sigma+\omega}$, the ρ meson V_ρ, and Coulomb potential V_{cou}.

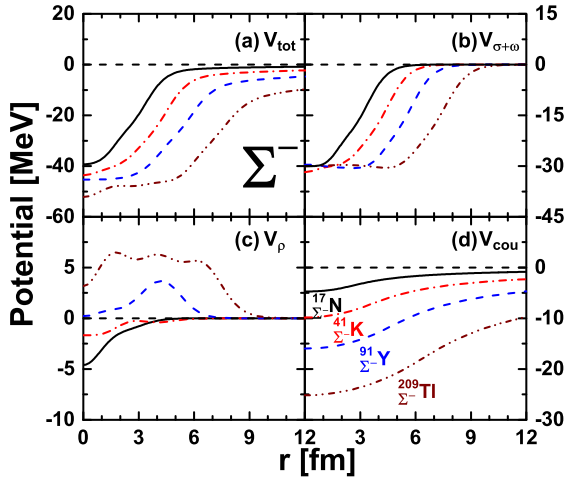

FIG. 8. The same as Fig. 7, but for the Σ^- hyperons in the hypernuclei ${}^{17}_{\Sigma^-}$N, ${}^{41}_{\Sigma^-}$K, ${}^{91}_{\Sigma^-}$Y, and ${}^{209}_{\Sigma^-}$Tl.

is mainly caused by the increasing repulsive Coulomb interaction. In particular, in the hypernucleus ${}^{209}_{\Sigma^+}$Bi, the Coulomb potential $V_{\rm cou}$ reaches as large as 26 MeV in the central part. The shallower potential will lead to more weakly bound s.p. levels. However, while the potentials become wider in heavier hypernuclei, more bound levels emerge. As a result, from ${}^{17}_{\Sigma^+}$F to ${}^{91}_{\Sigma^+}$Nb, the values of B_{Σ^+} for s and p orbits become larger, but B_{Σ^+} becomes smaller in ${}^{209}_{\Sigma^+}$Bi. Different from the Σ^+ hypernuclei, the mean-field potentials for the Σ^- hyperons become deeper from ${}^{17}_{\Sigma^-}$N to ${}^{209}_{\Sigma^-}$Tl due to the attractive Coulomb interaction. As with the Σ^+ hyperons, the potentials become wider with increasing mass number. All these changes will make s.p. levels more bound. The potentials contributed from the ρ meson V_ρ are completely opposite for the Σ^- and Σ^+ hyperons because of their opposite signs of the isospin third component, i.e., $\tau_{\Sigma^+,3} = +1$ and $\tau_{\Sigma^-,3} = -1$.

V. SUMMARY

Within the framework of RMF model, the single-hyperon ($Y = \Lambda$, $\Xi^{0,-}$, and $\Sigma^{-,0,+}$) hypernuclei are studied systematically. Detailed formalism for those hypernuclei in RMF model are presented. For the NN interaction, the PK1 parameter is adopted. For the YN interactions, parameters are constrained according to the experimental data or previous theoretical efforts. Among them, ΛN interaction is fixed by reproducing the experimental single-Λ binding energy $B_\Lambda^{(1s)}$ of the $1s$ orbit in hypernucleus ${}^{40}_{\Lambda}$Ca [83], the ΞN interaction is determined by fitting the observed Ξ^- removal energy in ${}^{15}_{\Xi^-}$C [80], and ΣN interaction is taken as in Ref. [57]. This work mainly includes three parts.

First, taking hypernuclei ^{40}Ca $+ Y(Y = \Lambda,\ \Xi^{0,-},\ \Sigma^{+,0,-})$ as examples, we investigate the mean-field potentials, single-hyperon levels, density distributions, and binding energies, where the consequences of introducing different types of hyperons are examined. We found that the mean-field potentials and the corresponding s.p. levels for the Λ and Σ^0 hyperons are very similar, because both of them are electroneutral and have very close coupling strengths with the σ and ω mesons. The Ξ^0 is the most weakly bound for which the density distributions is the most extended. Coulomb interactions play important roles in the Ξ^-, Σ^-, and Σ^+ hyperons, which causes the mean-field potential to be much shallower for positively charged Σ^+ hyperons while much deeper for the negatively charged Ξ^- and Σ^- hyperons. By comparing the binding energies and rms radii between ^{40}Ca and ^{40}Ca $+ Y$, the impurity effects from the single hyperon on the nuclear core are also studied. It is found that the intruded single hyperon makes the nuclear system more bound, due to the attractive NY interaction. However, very different effects on the nucleon radii are observed for different hyperons. For example, for the neutron rms radius R_n, Ξ^0 and Σ^+ hyperons decrease R_n, Ξ^- and Σ^- hyperons increase R_n, and Λ and Σ^0 hyperons have almost no influence on R_n. Unlike the case of R_n, the Coulomb interaction is important for the proton radius R_p and charge radius R_c. For example, the positively charged Σ^+ increases R_p and R_c while the negatively charged hyperon Ξ^- and Σ^- make them smaller.

Second, taking ^{40}Ca $+ Y(Y = \Lambda,\ \Xi^{0,-},\ \Sigma^{+,0,-})$ as examples, the ωYY tensor couplings and the effects on the single-hyperon levels are studied. In general, the ωYY tensor couplings obviously influence the spin-orbit splittings but have different effects for different hyperons. For the Λ and $\Xi^{0,-}$ hyperons, the ωYY tensor potentials reduce the spin-orbit splittings, while for the $\Sigma^{+,0,-}$ hyperons they are increased. In particular, for the $\Xi^{0,-}$ hyperons, the level ordering is inverted by large ωYY tensor potential.

Finally, taking ^{16}O $+ Y$, ^{40}Ca $+ Y$, ^{90}Zr $+ Y$, and ^{208}Pb $+ Y$ as examples, the mass dependence of the single-hyperon binding energies are studied. Generally, the binding energy increases with the mass number A for all hyperons. In different hypernuclei, the values of single-hyperon binding energies are very different. For examples, for the Σ^- hyperon, B_Y of the $1s$ orbit reaches as much as 40 MeV in ^{208}Pb $+ \Sigma^-$, but it is only half of that for Ξ^0 hyperons. In the same manner, the number of bound levels is very different. Furthermore, there is a turning point for Σ^+ hyperon where the binding energy decreases after ${}^{91}_{\Sigma^+}$Nb, which is mainly caused by the repulsive Coulomb interaction.

ACKNOWLEDGMENTS

This work was partly supported by the Physics Research and Development Program of Zhengzhou University (Grant No. 32410017) and the National Natural Science Foundation of China (Grants No. 11175002, No.11335002, No. 11375015, No. 11505157, No. 11705163, and 11775119).

[1] M. Danysz and J. Pniewski, Philos. Mag. **44**, 348 (1953).
[2] O. Hashimoto and H. Tamura, Prog. Part. Nucl. Phys. **57**, 564 (2006).
[3] A. Feliciello and T. Nagae, Rep. Prog. Phys. **78**, 096301 (2015).
[4] A. Gal, E. V. Hungerford, and D. J. Millener, Rev. Mod. Phys. **88**, 035004 (2016).

[5] T. Nagae, Prog. Theor. Phys. Suppl. **185**, 299 (2010).
[6] J. Hao, T. T. S. Kuo, A. Reuber, K. Holinde, J. Speth, and D. J. Millener, Phys. Rev. Lett. **71**, 1498 (1993).
[7] Z.-Y. Ma, J. Speth, S. Krewald, B.-Q. Chen, and A. Reuber, Nucl. Phys. A **608**, 305 (1996).
[8] Y. Tzeng, S. Y. Tsay Tzeng, and T. T. S. Kuo, Phys. Rev. C **65**, 047303 (2002).
[9] E. Hiyama, T. Motoba, T. A. Rijken, and Y. Yamamoto, Prog. Theor. Phys. Suppl. **185**, 1 (2010).
[10] J. Schaffner-Bielich, Nucl. Phys. A **804**, 309 (2008).
[11] I. Vidaña, Nucl. Phys. A **914**, 367 (2013).
[12] X. Y. Xing, J. N. Hu, and H. Shen, Phys. Rev. C **95**, 054310 (2017).
[13] T.-T. Sun, C.-J. Xia, S.-S. Zhang, and M. S. Smith, Chin. Phys. C **42**, 025101 (2018).
[14] Y. Zhang, J. N. Hu, and P. Liu, Phys. Rev. C **97**, 015805 (2018).
[15] H. Hotchi, T. Nagae, H. Outa, H. Noumi, M. Sekimoto, T. Fukuda, H. Bhang, Y. D. Kim, J. H. Kim, H. Park *et al.*, Phys. Rev. C **64**, 044302 (2001).
[16] F. Garibaldi, O. Hashimoto, J. J. LeRose, P. Markowitz, S. N. Nakamura, J. Reinhold, and L. Tang, J. Phys: Conf. Ser. **299**, 012013 (2011).
[17] R. S. Hayano, T. Ishikawa, M. Iwasaki, H. Outa, E. Takada, H. Tamura, A. Sakaguchi, M. Aoki, and T. Yamazaki, Phys. Lett. B **231**, 355 (1989).
[18] D. J. Prowse, Phys. Rev. Lett. **17**, 782 (1966).
[19] M. Danysz, K. Garbowska, J. Pniewski, T. Pniewski, J. Zakrzewski, E. R. Fletcher, J. Lemonne, P. Renard, J. Sacton, W. T. Toner *et al.*, Nucl. Phys. **49**, 121 (1963).
[20] S. Aoki, S. Y. Bahk, K. S. Chung, S. H. Chung, H. Funahashi, C. H. Hahn, T. Hara, S. Hirata, K. Hoshino, M. Ieiri *et al.*, Prog. Theor. Phys. **85**, 1287 (1991).
[21] P. Khaustov, D. E. Alburger, P. D. Barnes, B. Bassalleck, A. R. Berdoz, A. Biglan, T. Bürger, D. S. Carman, R. E. Chrien, C. A. Davis *et al.*, Phys. Rev. C **61**, 054603 (2000).
[22] S. Aoki, S. Y. Bahk, K. S. Chung, S. H. Chung, H. Funahashi, C. H. Hahn, T. Hara, S. Hirata, K. Hoshino, M. Ieiri *et al.*, Prog. Theor. Phys. **89**, 493 (1993).
[23] K. Nakazawa, Y. Endo, S. Fukunaga, K. Hoshino, S. H. Hwang, K. Imai, H. Ito, K. Itonaga, T. Kanda, M. Kawasaki *et al.*, Prog. Theor. Exp. Phys. **2015**, 033D02 (2015).
[24] T. Motoba, H. Bandō, and K. Ikeda, Prog. Theor. Phys. **70**, 189 (1983).
[25] E. Hiyama, M. Kamimura, K. Miyazaki, and T. Motoba, Phys. Rev. C **59**, 2351 (1999).
[26] E. Hiyama, M. Kamimura, Y. Yamamoto, and T. Motoba, Phys. Rev. Lett. **104**, 212502 (2010).
[27] J. Žofka, Czech. J. Phys. B **30**, 95 (1980).
[28] X.-R. Zhou, H.-J. Schulze, H. Sagawa, C.-X. Wu, and E.-G. Zhao, Phys. Rev. C **76**, 034312 (2007).
[29] M. T. Win and K. Hagino, Phys. Rev. C **78**, 054311 (2008).
[30] B.-N. Lu, E.-G. Zhao, and S.-G. Zhou, Phys. Rev. C **84**, 014328 (2011).
[31] M. Isaka, M. Kimura, A. Doté, and A. Ohnishi, Phys. Rev. C **87**, 021304 (2013).
[32] B.-N. Lu, E. Hiyama, H. Sagawa, and S.-G. Zhou, Phys. Rev. C **89**, 044307 (2014).
[33] E. Hiyama, M. Kamimura, T. Motoba, T. Yamada, and Y. Yamamoto, Phys. Rev. C **53**, 2075 (1996).
[34] J. M. Yao, Z. P. Li, K. Hagino, M. T. Win, Y. Y. Zhang, and J. Meng, Nucl. Phys. A **868**, 12 (2011).
[35] K. Hagino, J. M. Yao, F. Minato, Z. P. Li, and M. T. Win, Nucl. Phys. A **914**, 151 (2013).
[36] X.-R. Zhou, A. Polls, H.-J. Schulze, and I. Vidaña, Phys. Rev. C **78**, 054306 (2008).
[37] H.-F. Lü and J. Meng, Chin. Phys. Lett. **19**, 1775 (2002).
[38] H.-F. Lü, J. Meng, S. Q. Zhang, and S.-G. Zhou, Eur. Phys. J. A **17**, 19 (2003).
[39] C.-Y. Song and J.-M. Yao, Chin. Phys. C **34**, 1425 (2010).
[40] C.-Y. Song, J. M. Yao, H. F. Lü, and J. Meng, Int. J. Mod. Phys. E **19**, 2538 (2010).
[41] C.-Y. Song, J. M. Yao, and J. Meng, Chin. Phys. Lett. **28**, 92101 (2011).
[42] H. Z. Liang, J. Meng, and S.-G. Zhou, Phys. Rep. **570**, 1 (2015).
[43] W.-L. Lu, Z.-X. Liu, S.-H. Ren, W. Zhang, and T.-T. Sun, J. Phys. G: Nucl. Part. Phys. **44**, 125104 (2017).
[44] T. Motoba, H. Bandō, K. Ikeda, and T. Yamada, Prog. Theor. Phys. Suppl. **81**, 42 (1985).
[45] H. Bandō, T. Motoba, and J. Žofka, Int. J. Mod. Phys. A **05**, 4021 (1990).
[46] A. Gal, J. M. Soper, and R. H. Dalitz, Ann. Phys. (NY) **63**, 53 (1971).
[47] R. H. Dalitz and A. Gal, Ann. Phys. (NY) **116**, 167 (1978).
[48] D. J. Millener, Nucl. Phys. A **804**, 84 (2008).
[49] M. Isaka, M. Kimura, A. Dote, and A. Ohnishi, Phys. Rev. C **83**, 044323 (2011).
[50] M. Rayet, Ann. Phys. (NY) **102**, 226 (1976).
[51] M. Rayet, Nucl. Phys. A **367**, 381 (1981).
[52] Y. Yamamoto, H. Bandō, and J. Žofka, Prog. Theor. Phys. **80**, 757 (1988).
[53] M. T. Win, K. Hagino, and T. Koike, Phys. Rev. C **83**, 014301 (2011).
[54] R. Brockmann and W. Weise, Phys. Lett. B **69**, 167 (1977).
[55] A. Bouyssy, Phys. Lett. B **99**, 305 (1981).
[56] N. K. Glendenning, D. Von-Eiff, M. Haft, H. Lenske, and M. K. Weigel, Phys. Rev. C **48**, 889 (1993).
[57] J. Mareš and B. K. Jennings, Phys. Rev. C **49**, 2472 (1994).
[58] Y. Sugahara and H. Toki, Prog. Theor. Phys. **92**, 803 (1994).
[59] D. Vretenar, W. Pöschl, G. A. Lalazissis, and P. Ring, Phys. Rev. C **57**, R1060 (1998).
[60] H. Shen, F. Yang, and H. Toki, Prog. Theor. Phys. **115**, 325 (2006).
[61] R. Wirth, D. Gazda, P. Navrátil, A. Calci, J. Langhammer, and R. Roth, Phys. Rev. Lett. **113**, 192502 (2014).
[62] B. D. Sert and J. D. Walecka, Adv. Nucl. Phys. **16**, 1 (1986).
[63] P.-G. Reinhard, Rep. Prog. Phys. **52**, 439 (1989).
[64] P. Ring, Prog. Part. Nucl. Phys. **37**, 193 (1996).
[65] D. Vretenar, A. V. Afanasjev, G. A. Lalazissis, and P. Ring, Phys. Rep. **409**, 101 (2005).
[66] J. Meng, H. Toki, S.-G. Zhou, S. Q. Zhang, W. H. Long, and L. S. Geng, Prog. Part. Nucl. Phys. **57**, 470 (2006).
[67] J. Meng and S.-G. Zhou, J. Phys. G: Nucl. Part. Phys. **42**, 093101 (2015).
[68] T.-T. Sun, Sci. Sin.-Phys. Mech. Astron. **42**, 012006 (2016).
[69] W. Zhang and Y.-F. Niu, Chin. Phys. C **41**, 094102 (2017).
[70] W. Zhang and Y. F. Niu, Phys. Rev. C **96**, 054308 (2017).
[71] W. Zhang and Y. F. Niu, Phys. Rev. C **97**, 054302 (2018).
[72] W. Brückner, M. A. Faessler, T. J. Ketel, K. Kilian, J. Niewisch, B. Pietrzyk, B. Povh, H. G. Ritter, M. Uhrmacher, P. Birien *et al.*, Phys. Lett. B **79**, 157 (1978).
[73] J. Boguta and S. Bohrmann, Phys. Lett. B **102**, 93 (1981).

[74] M. Rufa, H. Stöcker, J. Maruhn, P.-G. Reinhard, and W. Greiner, J. Phys. G **13**, 143 (1987).
[75] M. Rufa, J. Schaffner, J. Maruhn, H. Stöcker, W. Greiner, and P.-G. Reinhard, Phys. Rev. C **42**, 2469 (1990).
[76] J. K. Zhang and X. J. Qui, Phys. Lett. B **152**, 153 (1985).
[77] M. Chiapparini, A. O. Gattone, and B. K. Jennings, Nucl. Phys. A **529**, 589 (1991).
[78] Y. S. Shen and Z. Z. Ren, Acta. Phys. Sin. (Overseas Ed.) **7**, 258 (1998).
[79] J. K. Bunta and Š. Gmuca, Phys. Rev. C **70**, 054309 (2004).
[80] T.-T. Sun, E. Hiyama, H. Sagawa, H.-J. Schulze, and J. Meng, Phys. Rev. C **94**, 064319 (2016).
[81] M. Bender, K. Rutz, P.-G. Reinhard, and J. A. Maruhn, Eur. Phys. J. A **7**, 467 (2000).
[82] W. H. Long, J. Meng, N. Van Giai, and S.-G. Zhou, Phys. Rev. C **69**, 034319 (2004).
[83] S.-H. Ren, T.-T. Sun, and W. Zhang, Phys. Rev. C **95**, 054318 (2017).
[84] C. B. Dover and A. Gal, Prog. Part. Nucl. Phys. **12**, 171 (1984).
[85] M. M. Nagels, T. A. Rijken, and J. J. de Swart, Phys. Rev. D **12**, 744 (1975).
[86] T.-T. Sun, W.-L. Lu, and S.-S. Zhang, Phys. Rev. C **96**, 044312 (2017).